Thermoelectric Cu-S based materials synthesized via scalable mechanochemical process

Peter Baláž, Marcela Achimovičová, Matej Baláž, Kan Chen, Oleksandr Dobrozhan, Emmanuel Guilmeau, Jiří Hejtmánek, Karel Knížek, Lenka Kubíčková, Petr Levinský, et al.

Thermoelectric Cu-S based materials synthesized via scalable mechanochemical process

Peter Baláž,[†] Marcela Achimovičová,[†] Matej Baláž,[†] Kan Chen,[‖] Oleksandr Dobrozhan,[‡] Emmanuel Guilmeau,[†‡] Jiří Hejtmánek,[§] Karel Knížek,[§] Lenka Kubíčková,[§,□] Petr Levinský,[§] Viktor Puchý,[#] Michael John Reece,[‖] Peter Varga,[&] and Ruizhi Zhang[‖]*

[†]Institute of Geotechnics, Slovak Academy of Sciences, Watsonova 45, Košice, 04001, Slovakia

[‡] Department of Electronics and Computer Technology, Sumy State University, Ryms'koho-Korsakova St. 2, Sumy, 40007, Ukraine

[†‡] CRISMAT, CNRS, Normandie University, ENSICAEN, UNICAEN, 6 Boulevard du Maréchal Juin, Caen, 14000, France

[§] Institute of Physics of the Czech Academy of Sciences, Cukrovarnická 112/10, Praha 6, 16200, Czechia

[□] Faculty of Mathematics and Physics, Charles University, V Holešovičkách 747/2, Praha 8, 18000 Czech Republic

[#] Institute of Materials Research, Slovak Academy of Sciences, Watsonova 47, Košice, 04001, Slovakia

‖ School of Engineering and Materials Science, Queen Mary University of London, Mile and Road, E1 4NS, London, United Kingdom

& TRATEC, s.r.o., Bratislavská 10, Prešov, 08001, Slovakia

Corresponding author
* E-mail: achimovic@saske.sk. Tel.: 00421-055-7922607.

ABSTRACT

In this work, Cu based sulfides (chalcopyrite $CuFeS_2$, mohite Cu_2SnS_3, tetrahedrite $Cu_{12}Sb_4S_{13}$, mawsonite $Cu_6Fe_2SnS_8$ and kesterite Cu_2ZnSnS_4) were synthesized by industrial milling in an excentric vibration mill to demonstrate scalability of their synthesis. For comparison, laboratory scale milling in a planetary mill was performed. The properties of the obtained samples were characterized by X-ray diffraction, and in some cases, also by Mössbauer spectroscopy. For densification of powders the method of Spark Plasma Sintering was applied to prepare suitable samples for thermoelectric (TE) characterization which created the core of this paper. Comparison of the figure-of-merit ZT, representative of the efficiency of thermoelectric performance, show that the scaling process of mechanochemical synthesis leads to the similar values than using laboratory methods. This makes the cost effective production of Cu-based sulfides as prospective energy materials for converting heat to electricity feasible. Several new concepts have been developed involving combinations of natural and synthetic species (tetrahedrite) and nanocomposite formation (tetrahedrite/digenite, mawsonite/stannite) offer sustainable approaches in solid state chemistry. Mechanochemical synthesis is selected as a simple, one-pot and facile solid-state synthesis of thermoelectric materials with the capability to reduce, or even eliminate solvents,

toxic gases, high temperatures with controllable enhanced yields. The synthesis is environmentally friendly and essentially waste-free. The obtained results illustrate the possibility of large-scale deployment of energy-related materials.

KEYWORDS: energy materials, thermoelectrics, multinary copper sulfides, mechanochemistry, scalable solid state synthesis

INTRODUCTION

Statistical results show that more than 60% of energy is lost in vain, most of it in the form of waste heat[1]. Over 80% of waste heat generated in industrial processes is in the temperature range of 100-300 °C, suggesting that considerable opportunities exist for the development of efficient thermoelectric materials that operate at this regime[2]. Thermoelectric devices offer a viable way to generate electricity from a temperature gradient without hazardous side products. They are silent, reliable, scalable, predictable and durable. However, their applications remain limited because the best-known materials for thermoelectric devices are based on scarce, toxic and costly compounds with limited chemical stability at operating conditions. For example, the abundance of telurium is only 0.001 ppm, which is significantly lower than silver and even lower than gold and platinum. Moreover, its toxicity is high[3].

Several new compounds have emerged recently with high thermoelectric performance. Among them, metal chalcogenides have attracted considerable attention as potential telurium-free alternatives[3, 4]. Especially copper chalcogenides appeared as potential candidates due to their advantages: earth abundant, low cost, and less toxic character of constituting components and high thermoelectric performance[1, 5-8].

As for the application of thermoelectric materials, the Seebeck coefficient (S), electrical conductivity (σ) and thermal conductivity (κ) are measured at different temperatures (T) to calculate the values of dimensionless figure-of-merit ZT:

$$ZT = S^2\sigma/\kappa \quad (1)$$

(κ) is a sum of lattice thermal conductivity κ_L and electronic thermal conductivity (κ_e). Its ZT value determines the efficiency of thermoelectric materials. To ensure a high voltage output large S is needed, while a high σ is needed to limit losses by Joule effect. To maintain a temperature gradient low κ value is required[9]. Additionally, thermoelectric devices are of interest because of their silent operation, reliability, scalability, predictability and durability. They are used in cases when cost and energy efficiency are not so important as energy availability[10]. However, their broader application is needed in future energy materials aimed to harvest waste heat and reduce of fossile fuels consumption[11].

In 1990s the nanostructure approaches were introduced and applied to thermoelectrics to enhance their ZT values[10, 12-18]. Moreover, when non-equilibrium procedures such as high-energy milling and/or mechanochemical synthesis (HEM/MS), melt spinning and self-sustaining heating synthesis was applied, delicate multiscale structures was obtained[18]. In the case of the application of HEM/MS[4, 19-26] combined with spark plasma sintering[27] the created nanostructures also contribute to scatter phonons and thus to suppress lattice thermal conductivity κ_L. Since the invention of HEM, large quantities of nanoparticles can be prepared[16].

In this work we thus describe the properties and thermoelectric performances of several copper-based multinary sulfides. This include chalcopyrite $CuFeS_2$, mohite Cu_2SnS_3, tetrahedrite $Cu_{12}Sb_4S_{13}$, mawsonite $Cu_6Fe_2SnS_8$ and kesterite Cu_2ZnSnS_4 synthesized from elements in an industrial mill[28]. After synthesis the produced powders were densified using spark plasma sintering (SPS) and eventually, hot pressing (HP) techniques–see SI. The

properties of the products were studied by several characterization techniques and their thermoelectric performances were evaluated.

MATERIALS AND METHODS

For mechanochemical synthesis of chalcopyrite $CuFeS_2$, mohite Cu_2SnS_3, tetrahedrite $Cu_{12}Sb_4S_{13}$, mawsonite $Cu_6Fe_2SnS_8$ and kesterite Cu_2ZnSnS_4, the following precursors were used: copper (Merck, 99% purity), antimony (Alpha Aesar, 99.5% purity), tin (Nihon Seiko, 99% purity), iron (Winlab, 99% purity), zinc (Aldrich, 99% purity), and sulfur (CG-Chemikalien, 99% purity). The elemental precursors for appropriate sulfides were mixed in stoichiometric amounts. In some cases natural minerals of chalcopyrite $CuFeS_2$ (deposit Zhezkazgan, Kazachstan[29] with the main admixture silicon oxide SiO_2 (JCPDS 01-077-1060)) and tetrahedrite $Cu_{12}Sb_4S_{13}$ (deposit Rožňava, Slovakia) with the main admixtures siderite $FeCO_3$ (JCPDS 01-083-1764) and silicon oxide SiO_2 (JCPDS 01-077-1060)) were used.

The syntheses were carried out in an industrial eccentric vibratory ball mill ESM 656-0.5ks (Siebtechnik, Germany) working under the following conditions: 5L steel satellite milling chamber attached to the main corpus of the mill, tungsten carbide balls with a diameter of 35 mm and total mass of 30 kg, 80% ball filling in milling chamber, amplitude of inhomogenous vibrations 20 mm, rotational speed of the eccenter 960 min^{-1}, argon atmosphere. The total feed of reaction precursors was 100 g per batch. The milling was performed for different times which are mentioned in the appropriate sections.

For comparison, the syntheses were also carried out in a laboratory scale planetary mill Pulverisette 6 (Fritsch, Germany) working under the following conditions: 250 mL tungsten carbide milling chamber, tungsten carbide balls with a diameter of 10 mm and total mass of 360 g, 80% ball filling in a milling chamber, revolutions of the milling chamber 550 rpm,

argon atmosphere. The total feed of reaction precursors was 5 g per batch. The milling was performed for different times which are mentioned in the appropriate section.

After completion of the milling programs, the resulting pulverized powders were shaped and densified using SPS apparatus (FCTHPD25, Germany), eventually hot pressing. Technical details are given in SI (Table S1). The final thickness of the pellets was around 3 mm with a geometrical density in excess of 95% of the crystallographic value.

The qualitative identification of the phase compositions was performed by XRD method. For the systems under study, several diffractometers were applied with the working conditions summarized in SI.

^{57}Fe Mössbauer spectroscopy was employed to clarify the magnetic ordering in chalcopyrite and to identify possible admixtures of other Fe-bearing compounds. To measure the ^{57}Fe Mössbauer spectra, the powder samples were pressed into tablets with tableting wax. The spectra were collected at room temperature and in a helium bath cryostat by Janis Research Company, Inc. (Woburn, MA, USA) at 4.2 K in the transmission mode using a ^{57}Co/Rh source. The calibration of velocities and isomer shift was performed with respect to an α-Fe foil at room temperature.

The electrical resistivity (ρ) and Seebeck coefficient (S) were measured simultaneously from ingots, from 300K up to 700 K under partial pressure of helium or pure N_2 flow using an ZEM-3 (Ulvac-Riko, Japan) and home made system. Also a commercial instrument LSR-3/110 (Linseis, Germany) working in the He atmosphere was used. The absolute precision and mutual veracity of above-mentioned thermoelectric measurements was verified in[30]. This enabled to confirm both the relevance of the measured data and their veracity using various apparatuses. LFA 457 apparatus (Netzsch, Germany) was used for measuring the thermal diffusivity under argon flow. The thermal conductivity (κ) was determined as the product of the geometrical density, the thermal diffusivity, and the theoretical heat capacity using the

Dulong-Petit approximation. The Wiedemann-Franz law, using a Lorenz number estimated from the relationship $L=1.5 + \exp(-|S|/116)$[31] was used to calculate the lattice thermal conductivity by subtracting the electronic contribution to the total thermal conductivity ($\kappa_L=\kappa-\kappa_e$). The estimated measurement uncertainities are around 6 % for the Seebeck coefficient, 8 % for the electrical resistivity, 11 % for the thermal conductivity, and 20 % for the figure-of-merit.

RESULTS AND DISCUSSION

Chalcopyrite $CuFeS_2$

Chalcopyrite $CuFeS_2$, composed of earth-abundant, non-toxic and inexpensive elements, is a mineral with tetrahedral-type structure. The structure can be considered as a double sphalerite cell in which two Zn atoms are replaced orderly by one Cu ion and one Fe ion. This ordered arrangement in the lattice is in tetrahedral coordination with sulfur. The lattice constants of this tetragonal cell are a=5.2914 Å, c=10.422 Å, with the c-axis nearly doubled[32]. However, the sulphur atoms displaces from the center of the bonded tetrahedron, because the Fe-S bond is stronger and more anisotropic than the Cu-S bond[33]. $CuFeS_2$ is known to be an antiferromagnetic semiconductor at ambient pressure. The charge carriers are p- or n-type depending on the samples, at high temperature the n-type conductivity dominates[34].

In this respect the chalcopyrite has been reported as an interesting n-type thermoelectric material with a reported value of ZT=0.2[35]. As n-type doping procedure several approaches can be used; among all we note (i) the Fe overstoichiometry in $Cu_{1-x}Fe_{1+x}S_2$ or the Cu^{1+} substitution by Tm^{2+} species (Zn, Pd, …) in $Cu_{1-x}Tm_xFeS_2$ leading to generation of conducting electrons due to compensation of excess positive charge on Cu sites and (ii) sulfur deficiency $CuFeS_{2-x}$, where S deficiency, linked with sulfur vaporization during synthesis/compaction process suppres lattice thermal conductivity and act as donor doping.

We underline that in case of chalcopyrite, which is semiconducting in nature, the optimized doping must be used to improve thermoelectric performance with higher ZT values[36-41].

The idea of this paper is, however, to document the viability of the industrial milling process followed by the hot press treatment of mechanochemically synthesized non-doped $CuFeS_2$ in comparison with powders synthesized in a laboratory mill. The methods of XRD and Mössbauer spectroscopy were applied for bulk characterization.

As determined by XRD, the most prominent impurity in our mechanochemically synthesized $CuFeS_2$ is pyrite FeS_2 (~2.4 %) for in laboratory-milled samples and bornite Cu_5FeS_4 (0.6-0.8 %) for both types of mechanochemical synthesis. The occurrence of these two marginal intermediate products is supported by their identification in the high temperature solid state synthesis[42]. Small amounts of tungsten carbide WC (1.8 %) from wear coming from milling balls was evidenced for the sample milled industrially for a much longer time (720 min) in comparison with 60 min for laboratory mill (Figure 1). The crystallite size of the powders is about 10 nm.

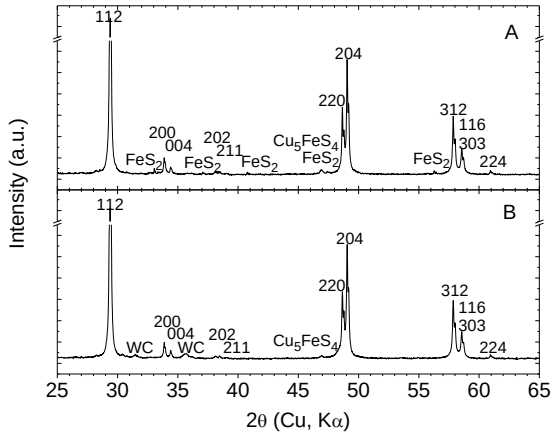

Figure 1. XRD spectra of chalcopyrite $CuFeS_2$, milling time: A-60 min (laboratory mill), B-720 min (industrial mill).

As we were interested in the impact of the mechanochemical synthesis on different scales on morphology and crystallinity of the synthesised powder material, we chose the Mössbauer

spectroscopy using ^{57}Fe nuclei as local probes for structural changes in chalcopyrite and for poorly crystalline admixtures. Since chalcopyrite is a strong antiferromagnet, its spectrum is characterised by Zeeman-split sextets (Figure 2), whose hyperfine parameters of these sextets correspond to tetrahedrally coordinated Fe^{3+} ions in the high spin state[43]. The broadening of the lines at low temperatures is caused by defects[44] introduced into the structure during the mechanochemical synthesis and can be accounted for by fitting by more components with different numbers of defects among the nearest neighbors of the Fe site[43]. Interestingly, the sample prepared in the laboratory mill has less defects than the one synthesized in the industrial mill, although the low-temperature spectrum of the latter indicates that a certain amount of the particles contains a highly crystalline core with bulk-like properties. The room-temperature spectra are further broadened by superparamagnetic relaxation of the nanoparticles with slightly slower Néel relaxation times than the time window of the method (10^{-7} s). In both samples, admixtures of pyrite (FeS_2) and iron oxyhydroxides (FeOOH) were found, however, the conditions in the laboratory mill produced the chalcopyrite phase of higher purity. The highly amorphous FeOOH, likely originating from water and oxygen adsorbed in the equipment, was not detected in XRD (Figure 1) and most probably forms a surface layer of the nanoparticles. To further elucidate the influence of the high-temperature treatment (e.g. hot pressing) on the morphology and composition of the samples Mössbauer spectroscopy will be performed for both hot-pressed samples as well. We suppose that the high-temperature treatment wil reduce the amount of the impurity phases together along with reduction of strain.

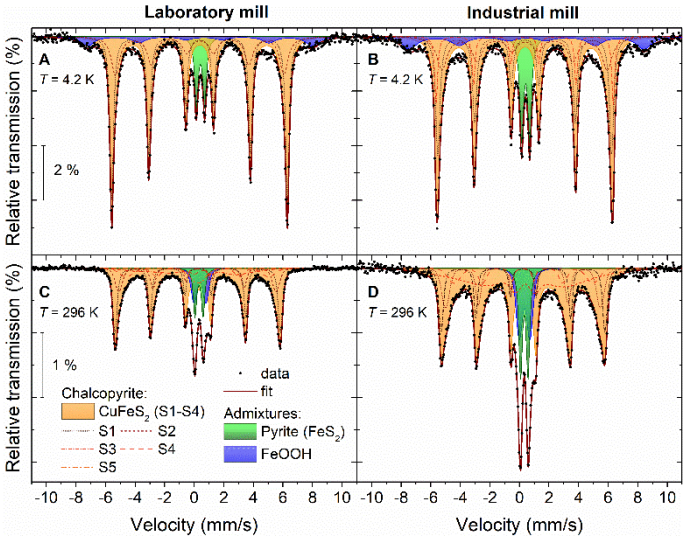

Figure 2. Mössbauer spectra of chalcopyrite $CuFeS_2$ measured at 4.2 K and 296 K, milling time: A, C-60 min (laboratory mill), B, D-720 min (industrial mill).

The temperature dependances of the electrical transport properties are shown in Figure 3a. Most importantly, both samples exhibit similar electric transport properties. The electrical resistivity perfectly reflects the semiconducting low-doped nature of synthesized $CuFeS_2$. The sign of Seebeck coefficient is changing from positive hole-like character at room temperature to negative electron-like behavior at higher temperatures (Figure 3b). The low concentration of point defects (acceptors and donors), in accordance with the variation of Seebeck coefficient, corresponds to an acceptor level accounting for p-type conductivity at low temperatures while a donor effect accounts for n-type conductivity at higher temperatures. This phenomenon is the same for both types of milling. The identical behaviour of both samples is documented also in the temperature dependence of their thermal conductivities, Figure 3c. Due to a very high electrical resistivity, the electronic contribution to the thermal conductivity is negligible. The observed substantially lower thermal conductivity compared with a pristine sample prepared by solid state reaction is due to nanostructuring of the sample. Similarly due to nanostructuration the low temperature “dielectric” peak, typical for “pure” crystallized insulators, is completely “depressed” as well as the high temperature values.

Here, due to substantially lower phonon mean free path of heat carrying phonons, the decrease of the thermal conductivity is likely due to increased scattering similar to "point defect" likely associated with the mechanochemical synthesis. The dependence of the figure-of-merit ZT on temperature is shown in Figure 3d. The ZT values for undoped $CuFeS_2$ are very low and of little significance for application. However, the key purpose of this study, is to demonstrate upgrading the milling process to an industrial scale, is clearly demonstrated. In this case, at 600 K the ZT value for an industrial milling is almost 2.5-times higher than in the case of a laboratory milling. Respecting the above-mentioned correlation between the doping and ZT optimization we refer to recent approach, where thermoelectric performance was enhanced by using non-doped $CuFeS_2$ nanocomposite created by co-milling of synthetic and natural species. An enhancement of the ZT values from 0.004 to 0.14 was obtained[29].

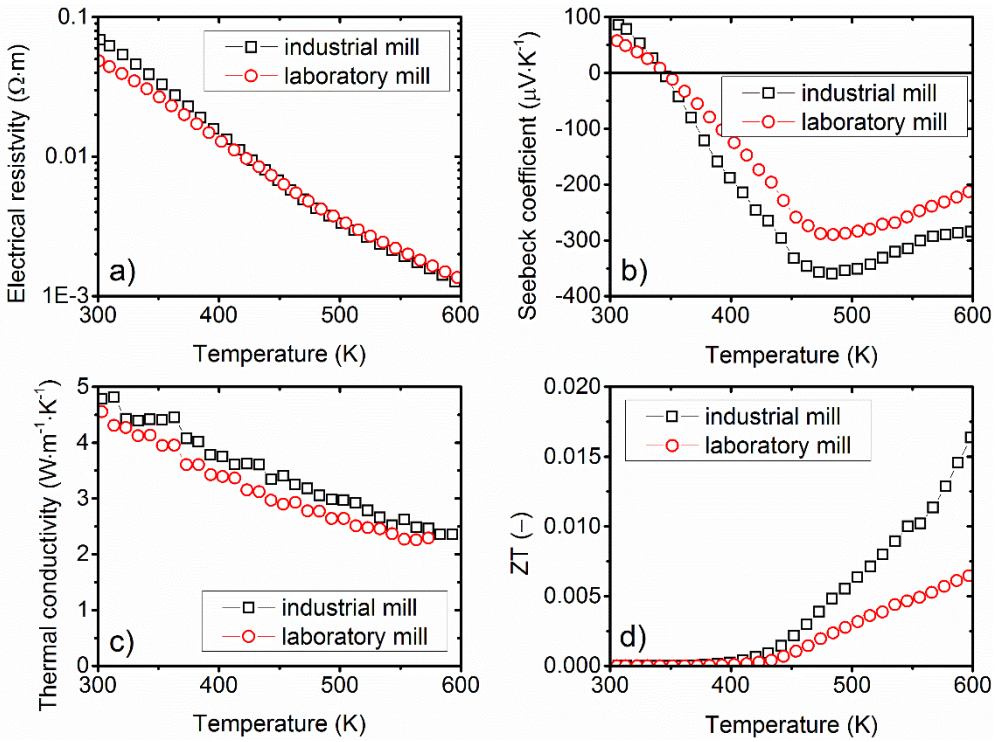

Figure 3. Thermoelectric performance of chalcopyrite $CuFeS_2$ as a function of temperature: a) electrical resistivity, b) Seebeck coefficient, c) thermal conductivity, d) figure-of-merit ZT. Milling time: laboratory mill-60 min, industrial mill-720 min.

Mohite Cu_2SnS_3

Cu_2SnS_3 belongs among ternary chalcogenides and is the most important representative of copper-tin-sulfur (CTS) family with mineralogical name mohite[45]. Already 4 polymorphs have been reported until now- tetragonal, monoclinic, cubic and trigonal[46-49]. Its main application field is photovoltaic[50], however, it has been also found as an interesting thermoelectric material[51-54]. The TE performance can be enhanced by doping with Mn[55], Fe[56], Zn[57], Co[58] and Ni[59]. There are many synthetic pathways to this compound, which can be divided into physical and chemical and have been nicely reviewed by Lokhande et al.[60, 61]. Mechanochemical synthesis representing a one-step environmentally friendly approach has also been used for the preparation of Cu_2SnS_3[54, 62-64]. Our research group has successfully prepared this compound from elements on a laboratory scale[65], and also from binary sulfides on a larger scale[66]. However, its application potential has not been revealed in our studies so far.

In the present study, we prepared CTS nanocrystals using mechanochemical synthesis in an eccentric vibratory mill. The XRD patterns of the elemental mixture of Cu, Sn and S taken after different time of milling are presented in Figure 4a. The XRD pattern of the powder mixture milled for 60 min already shows a significant amount of Cu_2SnS_3 product (either cubic or tetragonal polymorph). It is not possible to certainly determine the formed polymorph from the XRD patterns of the as-milled product with very broad peaks, as the main peaks of these phases are very close[49]. However, Lohani et al. who also used ball milling to prepare Cu_2SnS_3 nanocrystals (also starting from binary sulfides) reported the polymorph to be cubic[54]. In addition to the main phase, the non-reacted Sn and CuS could still be observed in the XRD pattern of the powders treated for 60 and 180 minutes. During the next 60 minutes, there was only a slight improvement of the progress of the reaction observed. The synthesis using the scaled-up process was much less rapid in comparison with planetary ball

milling using elemental precursors, which was reported to be finished in 15 minutes[65]. When using compounds, the process took longer, namely 60 and 240 min for planetary and eccentric vibratory milling, respectively[66]. The laboratory-scale planetary and scaled-up eccentric vibratory ball milling have been used also for other systems, e.g. kesterite[67, 68] and CuS synthesis[69, 70] and were directly compared in polyvinylchloride dechlorination using eggshell[71], always that showing much longer time is necessary when performing the eccentric vibratory milling.

Based on this analysis, the sample milled for 180 min was selected as an optimum one.

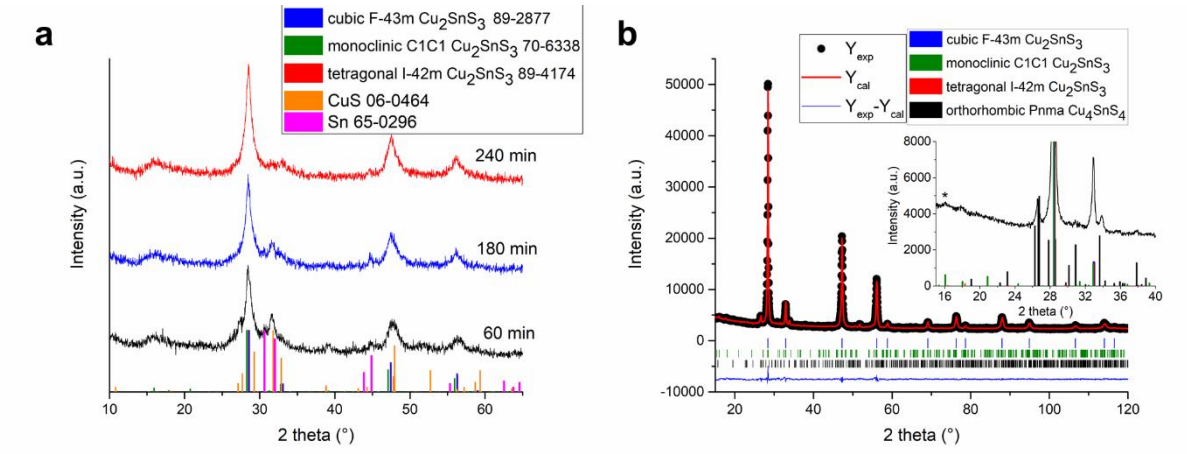

Figure 4. (a) XRD patterns of the Cu-Sn-S mixture milled for 60, 180 and 240 min in an eccentric vibratory mill and (b) the result of the Rietveld refinement of the XRD patterns of the reaction mixture milled for 180 min after spark plasma sintering (inset shows the zoomed 2 theta region between 15 and 40°). Rietveld factors are given in SI/Table S2. An asterisk described the probable presence of very small amounts of monoclinic phase.

In order to test the material for its potential applications in thermoelectrics, the as-received powder was subjected to spark plasma sintering at 550 °C. The XRD pattern of the sintered sample was subjected to Rietveld refinement and the result is shown in Figure 4b. We have

tried fitting the obtained XRD data in the tetragonal space group *I*-42m assigned to Cu_2SnS_3[54, 66], in monoclinic space group C1[47, 72] and also in cubic *F*-43m in[45]. The best fit has been obtained for the cubic phase, however, even better results were recorded when both cubic and monoclinic phase were considered, although the content of the latter was negligible. The lattice parameter a for the cubic phase was found to be 5.4314 ± 0.0002 Å, which is very close to the value 5.44 reported in[54,73]. The apparent crystallite size for the cubic Cu_2SnS_3 was found to be 288±55 nm and the observed strain was 0.2000±0.0229.

The 2 theta values at which the three main peaks were observed are 28.42°, 47.28° and 56.10°, allow which suggest the assignment of cubic *F*-43m space group rather than *I*-42m (by comparing the 2 theta values for both phases with those reported in[49]). The Cu_2SnS_3 in the same space group was reported by Lohani et al.[54]. In our case, also a very small amount of monoclinic phase is most probably present. The potential phase transformation from cubic/tetragonal to monoclinic structure should be supported by the presence of the peaks at lower 2θ values[54]. In Figure 4b, there is a very small diffraction peak at 16.1° marked with an asterisk, which could point to possible presence of the monoclinic phase. As the temperature of SPS was 550 °C, the cubic structure should be maintained to the large extent[49, 74]. Lohani et al. already observed 27% of the monoclinic phase after the treatment at this temperature[54].

The purity of the prepared material is quite high, with a very small amount of impurities denoted by the peaks located at 26.6° and 33.9°. The impurity has been identified as Cu_4SnS_4 phase, similarly to a previous study[66]. The thermoelectric properties of the sintered sample are displayed in Figure 5. The specific heat capacity was reported to be 0.44 J/gK[58], so this value has been used for further calculations.

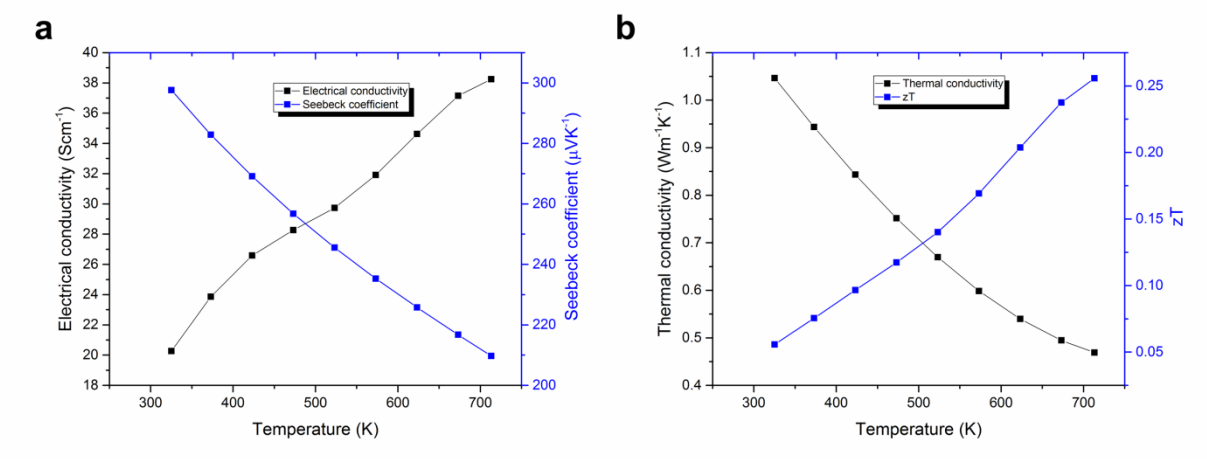

Figure 5. Thermoelectric performances of mohite Cu_2SnS_3 as a function of temperature, milling time-180 min (industrial mill): a)-electrical resistivity and Seebeck coefficient, b)-thermal conductivity and figure-of-merit ZT.

The thermoelectric properties of the planetary ball milled Cu_2SnS_3 have been recently reported in[54], showing the maximum ZT at 700 K to be around 0.3. We have obtained comparable result (ZT=0.26) using the scaled-up approach in this study, which further confirms that the disordered cubic *F*-43m structure has been obtained, although a small amount of monoclinic phase could slightly decrease the obtained ZT value. If the ordered monoclinic structure usually obtained at higher temperatures[74] was present, the TE properties should be significantly reduced, as nicely shown in[54]. In the literature, the ZT values at 700 K for undoped Cu_2SnS_3 nanocrystals are usually around 0.2 (this can be significantly enhanced by doping as shown in[55-59]). Thus the positive input of milling action both in terms of nanostructuring and defects formation is undeniable in our case. The combination of doping and mechanochemical synthesis might be an effective combination for further improvement of Cu_2SnS_3 thermoelectrics properties in the future.

Tetrahedrite $Cu_{12}Sb_4S_{13}$

Tetrahedrite as an Earth-abundant copper sulphide mineral with very low thermal conductivity[75] still represents continuous interest in the thermoelectric comunity[6, 8, 11, 76-78]. Moreover, its potential for application as energy material is currently expanding to be used also in photovoltaic devices[79, 80]. To enhance its thermoelectric performance, doping of mechanochemically synthesized $Cu_{12}Sb_4S_{13}$ is a promissing possibility as can be seen from papers published recently, see e.g.[81-85].

In this paper we present two innovative approaches for tetrahedrite:

1. *Mechanochemical synthesis: activation energy from electrical conductivity as a function of milling time*

We studied the temperature-dependent behavior of the electrical conductivity of synthetic tetrahedrite $Cu_{12}Sb_4S_{13}$ prepared by milling in an industrial mill for several different milling times. A detailed investigation of its properties is summarized in our recent paper[77]. By fitting the linear part of the relation $\ln(\sigma)=f(1/T)$, we determined the activation energies (E_a), which corresponds to three regimes of charge transport in milled samples (Figure 6a). At low temperatures (300-425 K) the activation energy changed in the range of E_a = 26-37 meV, to E_a=9-13 meV at medium temperatures (425-575 K), and to E_a =55-71 meV at high temperatures (575-700 K) (Figure 6b). These values of activation energy are similar to the results obtained for tetrahedrite systems reported earlier[86]. The behavior of charge transport in the low and medium regimes corresponds to semiconductor behavior, showing extrinsic nature due to the highly disordered character of the crystal structure of the milled samples and saturation modes. Moreover, we observed a behavior change at the higher temperatures, showing a semiconductor to metal transition in the intrinsic mode. This transition might be caused by conduction hopping effects in the energetic band gap of $Cu_{12}Sb_4S_{13}$ because of the excitation of minority charge carriers as observed in[87]. It is worth mentioning that depending on the milling time, the activation energies for three modes became almost saturated after 4

hours of milling with a slight decrease after 12 hours. The increase of the activation energy of carriers for three regimes can be attributed to the filling of the valence band which causes a decrease of the carrier concentration and leads to the decrease of the electrical conductivity[88, 89].

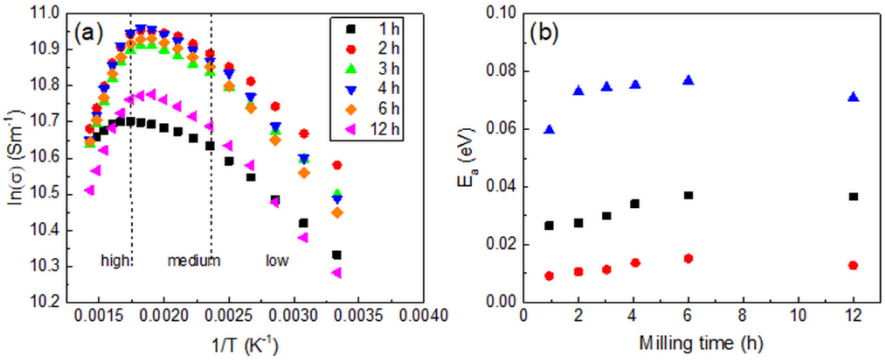

Figure 6. (a) Arrhenius dependence and (b) activation energy (E_a) as a function of the milling time for low (■), medium (●), and high (▲) temperature regimes, milling time 1-12 hours (industrial mill).

2. *Mechanochemical reduction: influence of composite formation during milling on thermoelectric performance*

Similarly to the ternary copper sulfide tetrahedrite $Cu_{12}Sb_4S_{13}$, binary copper sulfide digenite $Cu_{1.8}S$ (or Cu_9S_5), shows high values of figure of merit[3]. Digenite is a part of a large $Cu_{2-x}S$ family with end members chalcocite Cu_2S and covellite CuS. Within this family digenite has the highest power factor[90]. Digenite exhibits liquid-like behavior where Cu ion migration is the key to its high ZT values[8]. In copper metallurgy antimony-free digenite $Cu_{1.8}S$ is the desired product of $Cu_{12}Sb_4S_{13}$ decomposition because the presence of Sb worsens the properties of the final copper product. We developed a mechanochemical process for Sb removal from tetrahedrite by alkaline leaching (MELT) to produce digenite[91]. The simplified scheme behind the process can be described by hypothetical equation

$$3\ Cu_{12}Sb_4S_{13}(s) + 6\ Na_2S(l) \rightarrow 4\ Cu_9S_5(s) + 12\ NaSbS_2(l) \quad (2)$$

where (s)-solid phase, and (l)-liquid phase. The liquid phase can be separated and solid phase forms the $Cu_{12}Sb_4S_{13}/Cu_9S_5$ thermoelectric nanocomposite. By controlling the conversion degree of reaction (2), various ratio of both sulfides in nanocomposite can be obtained.

Based on this idea and considering our previous paper[77] where we demonstrated the possibility to synthesize non-doped tetrahedrite $Cu_{12}Sb_4S_{13}$ using an industrial mill we probed the robustness of this approach using combination both mechanochemically synthetized tetrahedrite and mechanically activated natural tetrahedrite. The combination of natural and synthetic tetrahedrites resembles the original works of Morelli´s group[92-94]. In their researches they applied *the mechanochemical synthesis* combining two tetrahedrites. However, the natural mineral with prevailing As over Sb was closer to the composition of tennantite $Cu_{12}As_4S_{13}$ than tetrahedrite. In our case *the mechanochemical reduction* according to reaction (2) creates nanocomposite of two different sulfides. After the original mineral tetrahedrite another efficient thermoelectric material formed is digenite. The samples under study are characterized in Table 1.

Table 1 Description of samples applied for thermoelectric performance

Sample	**Milling**	**Specification**
TELU 0	—	Natural tetrahedrite (mine Mária, Rožňava, Slovakia)
TELU 1	Laboratory mill (dry mode)	Milling of sample TELU 0
TELU 2	Laboratory mill (wet mode)	Milling of sample TELU 0
TELU 3	Industrial mill	Synthesis from elements for 2

	(dry mode)	hours, see[77]
TELU 4	Industrial mill (wet mode)	Co-milling of samples TELU 0 and TELU 3

The milling and leaching conditions of the samples listed in Table 1 are summarized in SI/2. Most importantly, the simulteneous milling and alkaline leaching should lead to modification of the thermoelectric parameters. In this respect we note that the use of natural tetrahedrite, with basically insulating character and relatively large power factor, represents a highly sensitive system that can unmask the role of electrically conducting extraneous phases via modification the thermoelectric response more clearly than highly electrically conducting matrix of ideal $Cu_{12}Sb_4S_{13}$. Our results are shown on Figure 7. In any case we underline that our study does not represent the final optimization approach enabling industrial transfer of natural tetrahedrite to an optimized p-type electronic material, nonetheless it shows the way how, the tetrahedrite mineral can be converted to a useful thermoelectrics using a low cost, effective and throughput route.

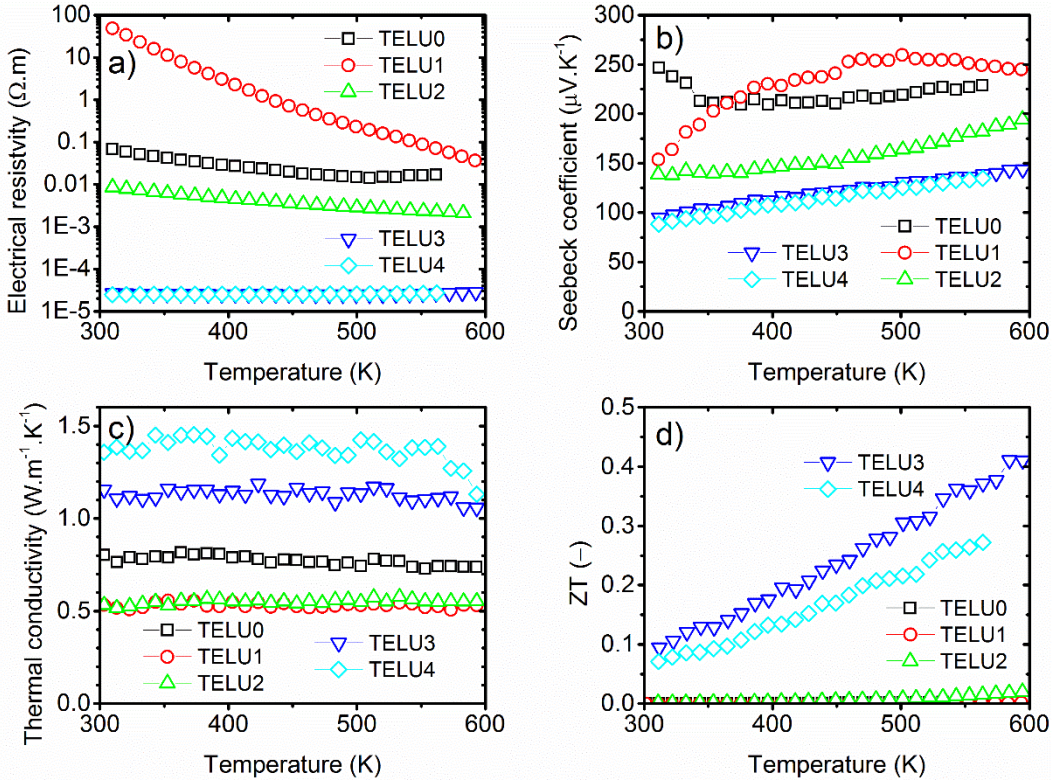

Figure 7. Thermoelectric performance as a function of temperature: a) electrical resistivity, b) Seebeck coefficient, c) thermal conductivity, d) figure-of-merit ZT.

Thermoelectric data acquired on natural tetrahedrite (TELU 0) revealed that the dry milling of natural tetrahedrite (all grains are under 200 microns) leads to a material with higher electrical resistivity and lower thermal conductivity compared to the mineral (Figures 7a and 7c). This can be attributed to increased interfacial scattering due to the grain size reduction (both defects and grain boundaries). The similar thermoelectric response, i.e. positive and weakly temperature dependent Seebeck coefficient of ~200 μV K^{-1} (Figure 7b), corroborates the semiconducting groundstate of the material.

Contrary to dry milling, the wet milling with application of leaching agent leads to a decrease of both electrical resistivity and Seebeck coefficient (Figures 7a and 7b) while the thermal conductivity retained the value of dry-milled sample (Figure 7c). The essentially modified electrical properties of the wet-milled sample are consistent with: (i) either modified

doping of original pristine phases or (ii) the introduction of an electrically conducting phase converting the resulting material into a composite where the electrical and thermoelectrical properties depend on the percolation behavior of the additional phase. In order to discern between these two possibilities we have intentionally performed long - term high temperature thermoelectric measurements that, in principle, unmask the role of percolation via electrically conducting precipitates as the short-time SPS sintering of the wet milled powder does not likely leads to a marked development of the conducting phase percolation network. Indeed, long-term high temperature measurements (5 days cycling between 300-700 K) led to a further decrease of the electrical resistivity (1.5 order of magnitude) and large decrease of the Seebeck coefficient at 300 K down to ~40 $\mu V\ K^{-1}$. Such low absolute values have never been observed even in highly doped tetrahedrites (S_{min}~ 65 $\mu V\ K^{-1}$ at 300 K) and therefore can only be explained by the presence of a "guest" phase in the "host" semiconducting tetrahedrite matrix, which rules out the possibility of milling-induced doping of natural tetrahedrite. Most importantly, based on the characteristic thermoelectric power of digenite $Cu_{1.8}S$ of ~ 30 $\mu V\ K^{-1}$ at 300 K and its large electrical conductivity[95, 96], we identify the minor phase in accord with equation (2) as a low amount of digenite $Cu_{1.8}S$ phase. The highly conducting $Cu_{1.8}S$ precipitates then create the percolation pathway in the semiconducting tetrahedrite matrix, which itself has high-temperature-dependent electrical resistance. The XRD analysis of the probed samples after SPS sintering showed that this treatment leads to the crystallite size between 60-100 nm. A careful XRD phase analysis of the TELU 2 sample confirmed the presence of a small concentration (~ 1-2%) of digenite in the as-prepared sample, whereas the $Cu_{1.8}S$ characteristic peaks were significantly more pronounced on the surface of the long-term high temperature annealed sample where the higher impact of the $Cu_{1.8}S$ phase was evidenced by thermoelectric measurements. In this respect we conclude that the simultaneous milling and alkaline leaching of non-doped semiconducting natural tetrahedrite is a viable

approach to modify the electronic properties via incorporation of highly conducting $Cu_{1.8}S$ species.

The samples labeled as TELU 3 and TELU 4 differ also by the procedure of ball milling, see Table 1. While TELU 3 was processed similarly as in our published paper[77], TELU 4 was processed by additional alkaline leaching in order to transform tetrahedrite to digenite, at least partly (see XRD pattern in SI/Figure S1). The comparative thermoelectric data, presented in Figures 7a-c, confirm that, contrary to the case of natural tetrahedrite with high electrical resistivity where small precipitate concentration can essentially influence the properties, the combination of industrially synthesized powder (TELU 3) and its subsequent chemical leaching in a planetary mill (TELU 4) does not lead to substantial modification of the robust thermoelectric properties. The polydisperse composites TELU 3 and TELU 4 posses properties defined by the dominating phase – tetrahedrite –shows similar thermal and transport properties: power factor between ~0.3 mW $m^{-1} K^{-2}$ (300 K) and ~0.65 mW $m^{-1} K^{-2}$ (500K) and weakly temperature dependent thermal conductivity between 1.1-1.4 W $m^{-1} K^{-1}$ at 300-800 K which results in ZT as already published, see Figure7d. We thus conclude that the industrial milling process, enabling the synthesis of $Cu_{12}Sb_4S_{13}$ based thermoelectrics, represents a robust technological route, highly durable and resilient towards undesirable chemical errors, while the intentional chemical leaching can be used to tune the thermoelectric response of insulating natural tetrahedrite.

Mawsonite $Cu_6Fe_2SnS_8$

The mineral mawsonite $Cu_6Fe_2SnS_8$ (MAW) belongs to sulfosalts of copper that occur in nature within hydrothermal copper deposits in altered volcanic rocks. It is frequently associated with other binary, ternary and quaternary sulfides. Recently, thirteen Cu-S based compounds as potential termoelectric materials were identified among which MAW was

mechanochemically synthesized for the first time in a laboratory mill[97]. The milling was performed for 96 hours and thermoelectric performance was evaluated. A figure-of-merit value ZT = 0.43 at 623 K was calculated. Thus the mineralogical curiosity named after Antarctic explorer Douglas Mawson started to interest the thermoelectric community in its effort to mimic natural minerals. Recently, the thermoelectric properties of MAW were thoroughly studied[98]. The authors in their theoretical work revealed that the low thermal conductivity of MAW is a consequence of low frequency vibration modes of Cu-ions. Good electronic transport properties and low thermal conductivity give promising thermoelectric performance characterized by a maximum ZT value of 0.5 at 750 K. However, up-scaling of MAW synthesis was documented only in our recent paper[99]. The mechanochemical solid state synthesis was performed for milling times of 5-240 min. The XRD analysis revealed that the transformation to final product proceeds via several intermediate steps where binary (CuS, SnS) and ternary (Cu_2SnS_3) sulfides were identified, and finally practically only MAW is present at milling for 240 min (Figure 8).

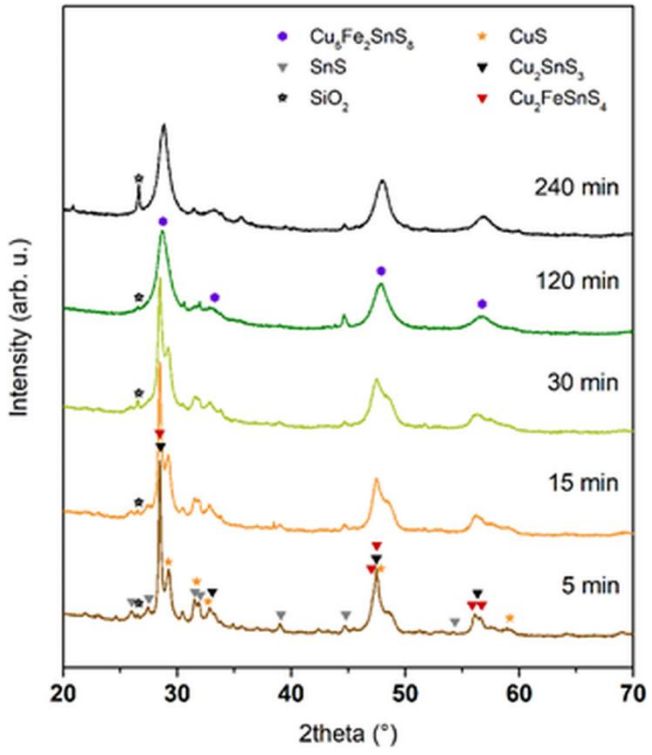

Figure 8. XRD patterns of reaction mixture after milling in an industrial mill (milling times are given on corresponding patterns). Reprinted by permission from **Copyright Clearance Center: Springer Nature, J. Electron. Mater., Mechanochemistry for Thermoelectrics: Nanobulk $Cu_6Fe_2SnS_8/Cu_2FeSnS_4$ Composite Synthesized in an Industrial Mill, Baláž, P.; Hegeduš, M.; Reece, M.; Zhang, R.; Su, T.; Škorvánek, I.; Briančin, J.; Baláž, M.; Mihálik, M.; Tešinský, M.; Achimovičová, M., 2019.**

Because of strong amorphization the identification of other phases is complicated. After densification by SPS the compacted sample milled for 240 min was re-measured by XRD and the pattern was processed by Rietveld refinement (Figure 9). Chalcopyrite $CuFeS_2$ and bornite Cu_5FeS_4 present as major impurities, were included into refinement calculations. However, the results with conventional Rietveld factor R_{wp} only over 22% were obtained. This led us to incorporate an other phase with structure closer to MAW for the calculations. After introduction of stannite Cu_2FeSnS_4, better results were obtained with R_{wp} = 12-13%. In conlusion to this analysis it is evident that MAW phase can be obtained by industrial milling only up to some content with the presence of secondary phase stannite. Despite phase impurity the obtained product is characterized by the good thermoelectric performance described below.

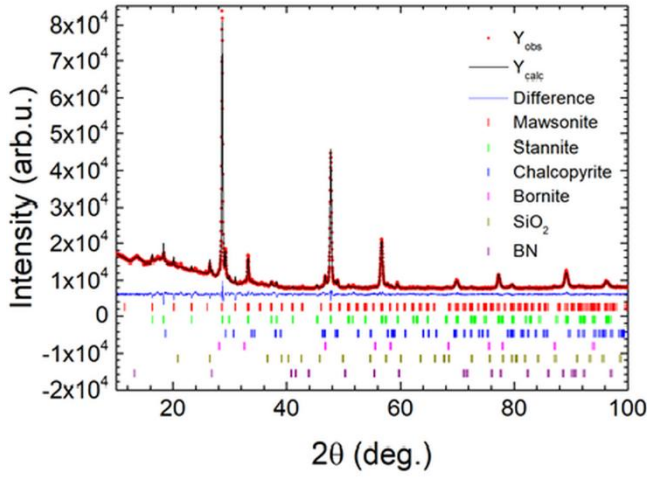

Figure 9. Rietveld analysis for the sample milled for 240 min in an industrial mill after SPS treatment. Rietveld factors are given in SI. Reprinted by permission from **Copyright Clearance Center: Springer Nature, J. Electron. Mater., Mechanochemistry for Thermoelectrics: Nanobulk $Cu_6Fe_2SnS_8/Cu_2FeSnS_4$ Composite Synthesized in an Industrial Mill, Baláž, P.; Hegeduš, M.; Reece, M.; Zhang, R.; Su, T.; Škorvánek, I.; Briančin, J.; Baláž, M.; Mihálik, M.; Tešinský, M.; Achimovičová, M., 2019.**

A summary of the thermoelectric measurements is shown in Figure 10. The relatively high value ZT of 0.51 at 623 K for industrially milled sample (Fig. 10f) results in a low lattice thermal conductivity 0.29 W mK^{-1} (Figure 10d) and moderate power factor 3.3 μW $cm^{-2}K^{-2}$ (Figure 10c). Especially the values of κ_L are encouraging because they are comparable with values for the top Cu-based sulfides such as colusite (0.3 W mK^{-1} at 663 K[100, 101] and tetrahedrite (0.2 W mK^{-1} at 673 K)[93].The electrical conductivity (Figure 10a) shows typical semiconducting behaviour. In previous work[97] this behaviour is discussed for laboratory milled sample as a consequence of Sn deficiency. It seems that this deficiency is greater in the industrially milled sample. In conclusion, the industrially synthesized mawsonite/stannite composite represents a perspective scalable energy material for future applications.

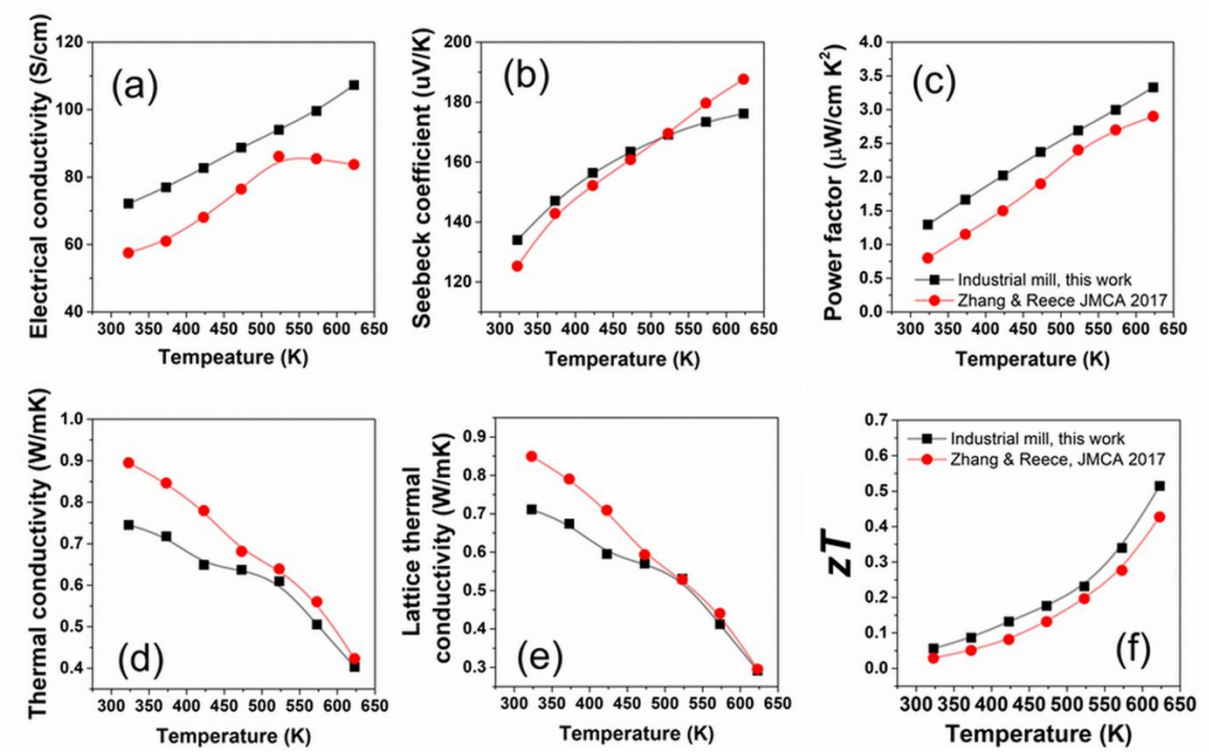

Figure 10. Thermoelectric performance for the samples milled 4 hours in an industrial mill and 96 hours in a laboratory mill (both after SPS treatment).

Kesterite Cu_2ZnSnS_4

Kesterite Cu_2ZnSnS_4 (CZTS) is recognized as a prominent material for photovoltaic applications. CZTS semiconductor has p-type conductivity, high absorption coefficients (~10^4-10^5 cm^{-1}) over the visible light wavelengths with an optical band gap (E_g~1.5 eV). It represents an environmentally friendly- and low-cost alternative to the currently used absorbers in photovoltaic cells[102]. Recently its potential application has been broadened to include thermoelectrics owing to its intrinsically low thermal conductivity[11, 103, 104].

Several synthesis routes for the preparation of CZTS have been evaluated. Among them, the mechanochemical synthesis starting from Cu, Zn, Sn and S elemental precursors demonstrates a scalable approach towards the pure CZTS nanocrystals[67, 68, 105]. The influence of changing

Cu:Zn ratio in Cu_2ZnSnS_4 leads to Cu/Zn disorder with consequences on its physical properties[106-109]. From a thermoelectric point this effect was analysed by[11]. Also, completely replacing Zn with Cu in Cu_2ZnSnS_4 will form Cu_3SnS_4, which has a disordered tetragonal structure with very low electrical resitivity[110]. It seems that non-stoichiometric compositions of $Cu_{2+x}Zn_{1-x}SnS_4$ is key to achieving an improvement of thermoelectric performance[104, 109].

Guided by the previously published work on kesterites, we selected several samples of industrially synthesized kesterites of which the photovoltaic properties have been reported[68] to perform thermoelectric measurements. With increasing milling time the samples became more amorphized and there was a gradual diminishing of the Zn peaks (Figure 11).

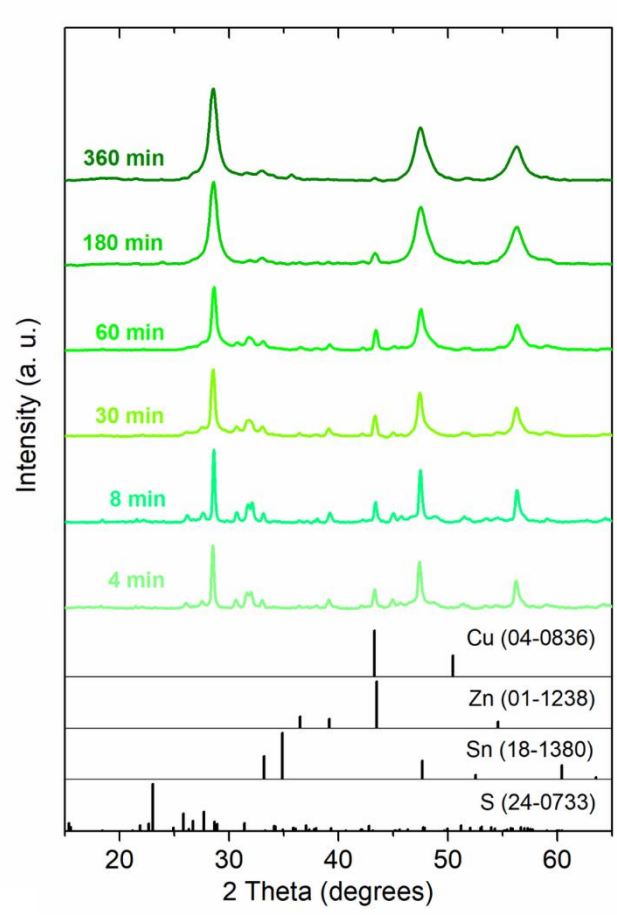

Figure 11. XRD pattern of reaction mixture after milling in an industrial mill (milling times are given on corresponding patterns). Reprinted by permission from **Copyright Clearance Center: John Wiley&Sons, Ltd., Photovolt. Res. Appl. Prog., Photovoltaic materials:**

Cu_2ZnSnS_4 (CZTS) nanocrystals synthesized via industrially scalable, green, one- step mechanochemical process, Baláž, P.; Hegeduš, M.; Baláž, M.; Daneu, N.; Siffalovič, P.; Bujňáková, Z.; Tóthová, E.; Tešinský, M.; Achimovičová, M.; Briančin, J.; Dutková, E.; Kaňuchová, M.; Fabián, M.; Kitazono, S.; Dobrozhan, O., 2019

After 360 minutes of milling, only the Bragg reflections assigned to the CZTS phase was identified[68], thus the as-received powder milled for 360 min was subjected to spark plasma sintering at 600 °C, in order to evaluate the materials thermoelectric related properties. The thermoelectric performance of this sample as a function of temperature is shown in Figure 12. It can be seen that the sample has relatively high resistivity and shows semiconducting behavior, as its electrical resistivity decreases with increasing temperature. It has a positive Seebeck coefficient indicating p-type conductivity. It is interesting to note that the Seebeck coefficient increased more rapidly in the temperature range of 475 - 525 K, which could be related to the order-disorder phase transition in kesterite. A similar temperature dependence of Seebeck was reported by Isotta[109]. The thermal conductivity decreases with increasing temperature, indicating phonon-phonon scattering as the main scattering effect and the sample shows low thermal conductivity. The sample shows a relatively low ZT value due to the fact that the electrical properties were not optimized. A similar ZT was reported in non-doped CZTS prepared by laboratory-scale mill[104]. The results indicate CZTS can be synthesized via industrial milling.

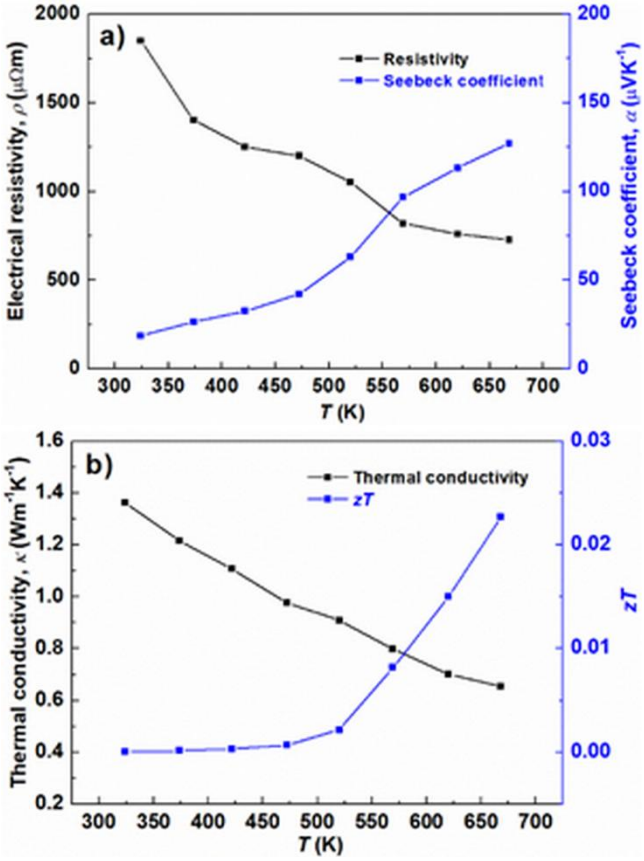

Figure 12. Thermoelectric performance of kesterite Cu_2ZnSnS_4 as a function of temperature, milling time - 360 min (industrial mill): a-electrical resistivity and Seebeck coefficient, b-thermal conductivity and figure-of-merit ZT.

CONCLUSION

In this work, Cu based sulfides (chalcopyrite $CuFeS_2$, mohite Cu_2SnS_3, tetrahedrite $Cu_{12}Sb_4S_{13}$, mawsonite $Cu_6Fe_2SnS_8$ and kesterite Cu_2ZnSnS_4 were synthesized by industrial milling in an excentric vibration mill. For comparison also laboratory scale milling in a planetary mill was performed. The properties of the obtained samples were characterized by X-ray diffraction and in special cases also by Mössbauer spectroscopy. For densification Spark Plasma Sintering or Hot Pressing was applied to prepare dense samples for thermoelectric measurements which created the core of this work. Values of the figure-of-merit ZT which is a measure of the efficiency of thermoelectric performance show that

scaling-up the process of mechanochemical synthesis leads to the similar values than using laboratory methods conditions (Table 2). This makes the production of Cu-based sulfides as a prospective energy harvesting material for converting heat to electricity feasible. Several new concepts have been developed, which especially a combination of natural and synthetic species (tetrahedrite) and nanocomposite formation (tetrahedrite/digenite, mawsonite/stannite) offer sustainable approaches in solid state chemistry. Mechanochemical synthesis and reduction is selected as a simple, one-pot and facile solid-state synthesis route for sulfide thermoelectric materials, with capability to reduce, or even eliminate solvents, toxic gases and the need of high temperatures with controllable enhanced yields. The synthesis of a large-scale nanostructured materials represents a major achievement in the field of nanotechnology. The synthesis is environmentally friendly and essentially waste-free. The obtained results illustrate the possibility of large-scale deployment of energy-related materials.

Table 2 Comparison of figure-of-merit ZT for sulfides under study.

Sulfide	Figure-of-merit ZT	
	Industrial milling	Laboratory milling
Chalcopyrite $CuFeS_2$	0.016@600 K[This work]*	0.007@600 K[This work]*
Mohite Cu_2SnS_3	0.26@713 K	0.30@723 K[54]
Tetrahedrite $Cu_{12}Sb_4S_{13}$	0.67@700 K[29]	0.65@673 K[93]
Mawsonite $Cu_6Fe_2SnS_8$	0.51@623 K[68]	0.43@623 K[97]
Kesterite Cu_2ZnSnS_4	0.023@673 K[This work]	0.04@673 K[109]

*Not optimized with repect to charge carrier concentration

ASSOCIATED CONTENT

Supporting Information

The Supporting Information is available free of charge at https://pubs.acs.org/doi/10.1021/....

and contains: experimental conditions of SPS treatment (Table S1), details about XRD measurements, milling conditions for tetrahedrite treatment for subsequent leaching, XRD pattern of tetrahedrite after leaching (Figure S1), and accuracy factors of the Rietveld refinement (Table S2).

ACKNOWLEDGEMENTS

This work was supported by the projects of the Slovak Grant Agency VEGA (2/0044/18, 2/0065/18), the Slovak Research and Development Agency APVV (VV-18-0357) and the Czech Science Foundation (18-12761S). The work was further supported by Operational Programme Research, Development and Education financed by European Structural and Investment Funds and the Czech Ministry of Education, Youth and Sport (SolidCZ.02.1.01/0.0/0.0/16_019/0000760).

References

1. Zhang, X.; Zhao, L., Thermoelectric materials: Energy Conversion between Heat and Electricity. *J. Materiomics* **2015,** *1* (2), 92-105. DOI:10.1016/j.jmat.2015.01.001
2. Long, S.; Powell, A.; Vaqueiro, P.; Hull, S., High Thermoelectric Performance of Bornite through Control of the Cu(II) Content and Vacancy Concentration. *Chem. Mater.* **2018,** *30* (2), 456-464. DOI:10.1021/acs.chemmater.7b04436
3. Ge, Z.; Zhao, L.; Wu, D.; Liu, X.; Zhang, B.; Li, J.; He, J., Low-cost, Abundant Binary Sulfides as Promising Thermoelectric Materials. *Mater. Today* **2016,** *19* (4), 227-239. DOI:10.1016/j.mattod.2015.10.004
4. Baláž, P.; Baláž, M.; Achimovičová, M.; Bujňáková, Z.; Dutková, E., Chalcogenide Mechanochemistry in Materials Science: Insight into Synthesis and Applications (a Review). *J Mater. Sci.* **2017,** *52* (20), 11851-11890. DOI:10.1007/s10853-017-1174-7
5. Suekuni, K.; Takabatake, T., Research Update: Cu-S Based Synthetic Minerals as Efficient Thermoelectric Materials at Medium Temperatures. *APL Mater.* **2016,** *4* (10). DOI:10.1063/1.4955398
6. Qiu, P.; Shi, X.; Chen, L., Cu-based Thermoelectric Materials. *Energy Storage Mater.* **2016,** *3*, 85-97. DOI:10.1016/j.ensm.2016.01.009

7. Li, J.; Pan, Y.; Wu, C.; Sun, F.; Wei, T., Processing of Advanced Thermoelectric Materials. *Sci. China-Technol. Sci.* **2017,** *60* (9), 1347-1364. DOI:10.1007/s11431-017-9058-8
8. Wei, T.; Qin, Y.; Deng, T.; Song, Q.; Jiang, B.; Liu, R.; Qiu, P.; Shi, X.; Chen, L., Copper Chalcogenide Thermoelectric Materials. *Sci. China-Mater.* **2019,** *62* (1), 8-24. DOI:10.1007/s40843-018-9314-5
9. Ioffe, A.F., *Semiconductor Thermoelements and Thermoelectric Cooling;* Infosearch Ltd.: London, 1956; pp 1-192.
10. Dresselhaus, M.; Chen, G.; Tang, M.; Yang, R.; Lee, H.; Wang, D.; Ren, Z.; Fleurial, J.; Gogna, P., New Directions for Low-dimensional Thermoelectric Materials. *Adv. Mater.* **2007,** *19* (8), 1043-1053. DOI:10.1002/adma.200600527
11. Powell, A., Recent Developments in Earth-abundant Copper-sulfide Thermoelectric Materials. *J. Appl. Phys.* **2019,** *126* (10), 100901-20. DOI:10.1063/1.5119345
12. Hicks, L.; Dresselhaus, M., Effect of Quantum-well Structures on the Thermoelectric Figure of Merit. *Phys. Rev. B* **1993,** *47* (19), 12727-2731. DOI:10.1103/PhysRevB.47.12727
13. Hicks, L.; Dresselhaus, M., Thermoelectric Figure of Merit of a One-dimensional Conductor. *Phys. Rev. B* **1993,** *47* (24), 16631-16634. DOI:10.1103/PhysRevB.47.16631
14. Vaqueiro, P.; Powell, A., Recent Developments in Nanostructured Materials for High-performance Thermoelectrics. *J. Mater. Chem.* **2010,** *20* (43), 9577-9584. DOI:10.1039/c0jm01193b
15. Kanatzidis, M.G., Nanostructured Thermoelectrics: the New Paradigm? *Chem. Mater.* **2010,** *22*, 648-659. DOI:10.1021/cm902195
16. Lan, Y.; Minnich, A.; Chen, G.; Ren, Z., Enhancement of Thermoelectric Figure-of-Merit by a Bulk Nanostructuring Approach. *Adv. Funct. Mater.* **2010,** *20* (3), 357-376. DOI:10.1002/adfm.200901512
17. Li, Z.; Xiao, C.; Zhu, H.; Xie, Y., Defect Chemistry for Thermoelectric Materials. *J. Am. Chem. Soc.* **2016,** *138* (45), 14810-14819. DOI:10.1021/jacs.6b08748
18. He, J.; Tritt, T., Advances in Thermoelectric Materials Research: Looking Back and Moving Forward. *Science* **2017,** *357*, 1369. DOI:10.1126/science.aak9997
19. Beyer, M.; Clausen-Schaumann, H., Mechanochemistry: The Mechanical Activation of Covalent Bonds. *Chem. Rev.* **2005,** *105* (8), 2921-2948. DOI:10.1021/cr030697h
20. Baláž, P., *Mechanochemistry in Nanoscience and Minerals Engineering;* Springer: Berlin, 2008; pp 1-413. DOI:10.1007/978-3-540-74855-7
21. Friscic, T., New Opportunities for Materials Synthesis Using Mechanochemistry. *J. Mater. Chem.* **2010,** *20* (36), 7599-7605. DOI:10.1039/c0jm00872a
22. Šepelák, V.; Becker, K., Mechanochemistry: from Mechanical Degradation to Novel Materials Properties. *J. Korean Ceram. Soc.* **2012,** *49* (1), 19-28. DOI: 10.4191/kcers.2012.49.1.019
23. Baláž, P.; Achimovičová, M.; Baláž, M.; Billik, P.; Cherkezova-Zheleva, Z.; Criado, J.; Delogu, F.; Dutková, E.; Gaffet, E.; Gotor, F.; Kumar, R.; Mitov, I.; Rojac, T.; Senna, M.; Streletskii, A.; Wieczorek-Ciurowa, K., Hallmarks of Mechanochemistry: from Nanoparticles to Technology. *Chem. Soc. Rev.* **2013,** *42* (18), 7571-7637. DOI: 10.1039/c3cs35468g
24. Do, J.; Friscic, T., Mechanochemistry: A Force of Synthesis. *ACS Central Sci.* **2017,** *3* (1), 13-19. DOI: 10.1021/acscentsci.6b00277
25. Mucsi, G., A Review on Mechanical Activation and Mechanical Alloying in Stirred Media Mill. *Chem. Eng. Res. Des.* **2019,** *148*, 460-474. DOI: 10.1016/j.cherd.2019.06.029
26. Friscic, T.; Mottillo, C.; Titi, H., Mechanochemistry for Synthesis. *Angewandte Chemie-Int. Ed.* **2020,** *59* (3), 1018-1029. DOI: 10.1002/anie.201906755

27. Bordia, R.; Kang, S.; Olevsky, E., Current Understanding and Future Research Directions at the Onset of the Next Century of Sintering Science and Technology. *J. Am. Ceram. Soc.* **2017,** *100* (6), 2314-2352. DOI: 10.1111/jace.14919
28. Gock, E.; Kurrer, K., Eccentric Vibratory Mills-Theory and Practice. *Powder Technol.* **1999,** *105* (1-3), 302-310. DOI: 10.1016/S0032-5910(99)00152-7
29. Baláž, P.; Dutková, E.; Levinský, P.; Daneu, N.; Kubíčková, L.; Knížek, K.; Baláž, M.; Navrátil, J.; Kašparová, J.; Ksenofontov, V.; Möller, A.; Hejtmánek, J., Enhanced Thermoelectric Performance of Chalcopyrite Nanocomposite via Co-milling of Synthetic and Natural Minerals. *Mater. Lett.* **2020,** *275*, 128107. DOI:10.1021/acs.chemmater.9b02637
30. Alleno, E.; Berardan, D.; Byl, C.; Candolfi, C.; Daou, R.; Decourt, R.; Guilmeau, E.; Hebert, S.; Hejtmanek, J.; Lenoir, B.; Masschelein, P.; Ohorodnichuk, V.; Pollet, M.; Populoh, S.; Ravot, D.; Rouleau, O.; Soulier, M., A Round Robin Test of the Uncertainty on the Measurement of the Thermoelectric Dimensionless Figure of Merit of $Co_{0.97}Ni_{0.03}Sb_3$. *Rev. Sci. Instrum.* **2015,** *86* (1), 011301-9. DOI: 10.1063/1.4905250
31. Kim, H.; Gibbs, Z.; Tang, Y.; Wang, H.; Snyder, G., Characterization of Lorenz Number with Seebeck Coefficient Measurement. *APL Mater.* **2015,** *3*, 041506-5. DOI: 10.1063/1.4908244
32. Habashi, F., *Chalcopyrite its Chemistry and Metallurgy;* Mc-Graw Hill: New York, 1978; pp 1-165. DOI:
33. Li, Y.; Zhang, T.; Qin, Y.; Day, T.; Snyder, G.; Shi, X.; Chen, L., Thermoelectric Transport Properties of Diamond-like $Cu_{1-x}Fe_{1+x}S_2$ Tetrahedral Compounds. *J. Appl. Phys.* **2014,** *116*, 203705-8. DOI: 10.1063/1.4902849
34. Teranishi, T., Magnetic and Electric Properties of Chalcopyrite. *J. Phys. Soc. Jpn.* **1961,** *16* (10), 1881-1887. DOI: 10.1143/JPSJ.16.1881
35. Li, J.; Tan, Q.; Li, J., Synthesis and Property Evaluation of $CuFeS_{2-x}$ as Earth-abundant and Environmentally-friendly Thermoelectric Materials. *J. Alloy. Compd.* **2013,** *551*, 143-149. DOI: 10.1016/j.jallcom.2012.09.067
36. Tsujii, N.; Meng, F.; Tsuchiya, K.; Maruyama, S.; Mori, T., Effect of Nanostructuring and High-Pressure Torsion Process on Thermal Conductivity of Carrier-doped Chalcopyrite. *J. Electron. Mater.* **2016,** *45* (3), 1642-1647. DOI: 10.1007/s11664-015-4147-0
37. Tsujii, N., Possible Enhancement of Thermoelectric Properties by Use of a Magnetic Semiconductor: Carrier-doped Chalcopyrite $Cu_{1-x}Fe_{1+x}S_2$. *J. Electron. Mater.* **2013,** *42* (7), 1974-1977. DOI: 10.1007/s11664-013-2485-3
38. Berthebaud, D.; Lebedev, O.; Maignan, A., Thermoelectric Properties of n-type Cobalt Doped Chalcopyrite $Cu_{1-x}Co_xFeS_2$ and p-type Eskebornite $CuFeSe_2$. *J. Materiomics* **2015,** *1* (1), 68-74. DOI: 10.1016/j.jmat.2015.03.007
39. Lefevre, R.; Berthebaud, D.; Mychinko, M.; Lebedev, O.; Mori, T.; Gascoin, F.; Maignan, A., Thermoelectric Properties of the Chalcopyrite $Cu_{1-x}M_xFeS_{2-y}$ Series (M = Mn, Co, Ni). *RSC Adv.* **2016,** *6* (60), 55117-55124. DOI: 10.1039/c6ra10046e
40. Vaure, L.; Liu, Y.; Cadavid, D.; Agnese, F.; Aldakov, D.; Pouget, S.; Cabotu, A.; Reiss, P.; Chenevier, P., Doping and Surface Effects of $CuFeS_2$ Nanocrystals Used in Thermoelectric Nanocomposites. *Chemnanomat* **2018,** *4* (9), 982-991. DOI: 10.1002/cnma.201800188
41. Navratil, J.; Kasparova, J.; Plechacek, T.; Benes, L.; Olmrova-Zmrhalova, Z.; Kucek, V.; Drasar, C., Thermoelectric and Transport Properties of n-type Palladium-Doped Chalcopyrite $Cu_{1-x}Pd_xFeS_2$ Compounds. *J. Electron. Mater.* **2019,** *48* (4), 1795-1804. DOI: 10.1007/s11664-018-06866-0

42. Xie, H.; Su, X.; Yan, Y.; Liu, W.; Chen, L.; Fu, J.; Yang, J.; Uher, C.; Tang, X., Thermoelectric Performance of $CuFeS_{2+2x}$ Composites Prepared by Rapid Thermal Explosion. *NPG Asia Mater.* **2017,** *9*, *e390*. DOI: 10.1038/am.2017.80
43. Tkáčová, K.; Baláž, P., Reactivity of Mechanically Activated Chalcopyrite. *Int. J. Miner. Process.* **1996,** *44-5*, 197-208.
44. Xie, H.; Su; X.; Zhang, X.; Hao, S.; Bailey, T.P.; Stoumpos, C.C.; Douvalis, A.P.; Hu, X.; Wolverton, C.; Dravid, V.P.; Uher, C.; Tang, X.; Kanatzidis, M. C., Origin of Intrinsically Low Thermal Conductivity in Talnakhite $Cu_{17.6}xFe_{17.6}S_{32}$ Thermoelectric Material: Correlations between Lattice Dynamics and Thermal Transport. *J. Am. Chem. Soc.* **2019,** *141*, 10905-10914. DOI:10.1021/jacs.9b05072
45. Kovalenker, V.A.; Malov, V.S.; Evstigneeva, T.L.; Vyaľsov, L.N., Mohite, Cu_2SnS_3, a New Sulphide of Tin and Copper. *Zapiski Vsesoyuznogo Mineralogicheskogo Obshchestva* **1982,** *111*, 110-114.
46. Dahman, H.; Rabaoui, S.; Alyamani, A.; El Mir, L., Structural, Morphological and Optical Properties of Cu_2SnS_3 Thin Film Synthesized by Spin Coating Technique. *Vacuum* **2014,** *101*, 208-211. DOI: 10.1016/j.vacuum.2013.08.019
47. Onoda, M.; Chen, X.; Sato, A.; Wada, H., Crystal Structure and Twinning of Monoclinic Cu_2SnS_3. *Mater. Res. Bull.* **2000,** *35* (9), 1563-1570. DOI: 10.1016/S0025-5408(00)00347-0
48. Han, J.; Zhou, Y.; Tian, Y.; Huang, Z.; Wang, X.; Zhong, J.; Xia, Z.; Yang, B.; Song, H.; Tang, J., Hydrazine Processed Cu_2SnS_3 Thin Film and their Application for Photovoltaic Devices. *Front. Optoelectronics* **2014,** *7* (1), 37-45. DOI: 10.1007/s12200-014-0389-3
49. Fernandes, P.; Salome, P.; da Cunha, A., A Study of Ternary Cu_2SnS_3 and Cu_4SnS_4 Thin Films Prepared by Sulfurizing Stacked Metal Precursors. *J. Phys. D* **2010,** *43*, 215403. DOI: 10.1088/0022-3727/43/21/215403
50. Reddy, V.; Pallavolu, M.; Guddeti, P.; Gedi, S.; Reddy, K.; Pejjai, B.; Kim, W.; Kotte, T.; Park, C., Review on Cu_2SnS_3, Cu_3SnS_4, and Cu_4SnS_4 Thin Films and their Photovoltaic Performance. *J. Ind. Eng. Chem.* **2019,** *76*, 39-74. DOI: 10.1016/j.jiec.2019.03.035
51. Shen, Y.; Li, C.; Huang, R.; Tian, R.; Ye, Y.; Pan, L.; Koumoto, K.; Zhang, R.; Wan, C.; Wang, Y., Eco-friendly p-type Cu_2SnS_3 Thermoelectric Material: Crystal Structure and Transport Properties. *Sci. Rep.* **2016,** *6*, 32501. DOI: 10.1038/srep32501
52. Nakamura, S.; Funabiki, H.; Shiga, S., Electrical Conductivity Improved Cu_2SnS_3 Thermoelectrics. *Phys. Status Solidi C* **2017,** *14* (6)**,** 1600162. DOI: 10.1002/pssc.201600172
53. Deng, T.; Qiu, P.; Song, Q.; Chen, H.; Wei, T.; Xi, L.; Shi, X.; Chen, L., Thermoelectric Properties of Non-stoichiometric $Cu_{2+x}Sn_{1-x}S_3$ Compounds. *J. Appl. Phys.* **2019,** *126*, 085111. DOI: 10.1063/1.5115195
54. Lohani, K.; Isotta, E.; Ataollahi, N.; Fanciulli, C.; Chiappini, A.; Scardi, P., Ultra-low Thermal Conductivity and Improved Thermoelectric Performance in Disordered Nanostructured Copper Tin Sulphide (Cu_2SnS_3, CTS). *J. Alloy. Compd.* **2020,** *830*, 154604. DOI: 10.1016/j.jallcom.2020.154604
55. Zhang, Z.; Zhao, H.; Wang, Y.; Hu, X.; Lyu, Y.; Cheng, C.; Pan, L.; Lu, C., Role of Crystal Transformation on the Enhanced Thermoelectric Performance in Mn-doped Cu_2SnS_3. *J. Alloy. Compd.* **2019,** *780*, 618-625. DOI: 10.1016/j.jallcom.2018.11.329
56. Zhao, L.; Chen, C.; Pan, L.; Hu, X.; Lu, C.; Wang, Y., Magnetic Iron Doping in Cu_2SnS_3 Ceramics for Enhanced Thermoelectric Transport Properties. *J. Appl. Phys.* **2019,** *125*, 095107. DOI: 10.1063/1.5065074
57. Zhou, W.; Shijimaya, C.; Takahashi, M.; Miyata, M.; Mott, D.; Koyano, M.; Ohta, M.; Akatsuka, T.; Ono, H.; Maenosono, S., Sustainable Thermoelectric Materials Fabricated by Using $Cu_2Sn_{1-x}Zn_xS_3$ Nanoparticles as Building Blocks. *Appl. Phys. Lett.* **2017,** *111*, 263105-5. DOI: 10.1063/1.5009594

58. Zhao, H.; Xu, X.; Li, C.; Tian, R.; Zhang, R.; Huang, R.; Lyu, Y.; Li, D.; Hu, X.; Pan, L.; Wang, Y., Cobalt-doping in Cu_2SnS_3: Enhanced Thermoelectric Performance by Synergy of Phase Transition and Band Structure Modification. *J. Mater. Chem. A* **2017,** *5* (44), 23267-23275. DOI: 10.1039/c7ta07140j
59. Xu, X.; Zhao, H.; Hu, X.; Pan, L.; Chen, C.; Li, D.; Wang, Y., Synergistic Role of Ni-doping in Electrical and Phonon Transport Properties of $Cu_2Sn_{1-x}Ni_xS_3$. *J. Alloy. Compd.* **2017,** *728*, 701-708. DOI: 10.1016/j.jallcom.2017.08.227
60. Lokhande, A.; Gurav, K.; Jo, E.; Lokhande, C.; Kim, J., Chemical Synthesis of Cu_2SnS_3 (CTS) Nanoparticles: A Status Review. *J. Alloy. Compd.* **2016,** *656*, 295-310. DOI: 10.1016/j.jallcom.2015.09.232
61. Lokhande, A.; Chalapathy, R.; He, M.; Jo, E.; Gang, M.; Pawar, S.; Lokhande, C.; Kim, J., Development of Cu_2SnS_3 (CTS) Thin Film Solar Cells by Physical Techniques: A Status Review. *Sol. Ener. Mat. Sol. C.* **2016,** *153*, 84-107. DOI: 10.1016/j.solmat.2016.04.003
62. Nomura, T.; Maeda, T.; Wada, T., Fabrication of Cu_2SnS_3 Solar Cells by Screen-printing and High-pressure Sintering Process. *Jpn. J. Appl. Phys.* **2014,** *53* (5), DOI: 10.7567/JJAP.53.05FW01
63. Neves, F.; Correia, J.; Hanada, K., Spark Plasma Sintering of Cu_2SnS_3 Powders Synthesized by Mechanical Alloying. *Mater. Lett.* **2016,** *164*, 165-168. DOI: 10.1016/j.matlet.2015.10.153
64. Vanalakar, S.; Agawane, G.; Shin, S.; Yang, H.; Patil, P.; Kim, J.; Kim, J., Non-vacuum Mechanochemical Route to the Synthesis of Cu_2SnS_3 Nano-ink for Solar Cell Applications. *Acta Mater.* **2015,** *85*, 314-321. DOI: 10.1016/j.actamat.2014.11.043
65. Baláž, M.; Daneu, N.; Rajňák, M.; Kurimský, J.; Hegeduš, M.; Dutková, E.; Fabián, M.; Kaňuchová, M.; Baláž, P., Rapid Mechanochemical Synthesis of Nanostructured Mohite Cu_2SnS_3 (CTS). *J. Mater. Sci.* **2018,** *53* (19), 13631-13642. DOI: 10.1007/s10853-018-2499-6
66. Hegeduš, M.; Baláž, M.; Tešinský, M.; Sayagues, M.; Siffalovič, P.; Kruľaková, M.; Kaňuchová, M.; Briančin, J.; Fabián, M.; Baláž, P., Scalable Synthesis of Potential Solar Cell Absorber Cu_2SnS_3 (CTS) from Nanoprecursors. *J. Alloy. Compd.* **2018,** *768*, 1006-1015. DOI: 10.1016/j.jallcom.2018.07.284
67. Hegeduš, M.; Baláž, P.; Baláž, M.; Siffalovič, P.; Daneu, N.; Kaňuchová, M.; Briančin, J.; Fabián, M., Mechanochemical Approach to a Cu_2ZnSnS_4 Solar Cell Absorber via a "Micro-nano" Route. *J. Mater. Sci.* **2018,** *53* (19), 13617-13630. DOI: 10.1007/s10853-018-2228-1
68. Baláž, P.; Hegeduš, M.; Baláž, M.; Daneu, N.; Siffalovič, P.; Bujňáková, Z.; Tóthová, E.; Tešinský, M.; Achimovičová, M.; Briančin, J.; Dutková, E.; Kaňuchová, M.; Fabián, M.; Kitazono, S.; Dobrozhan, O., Photovoltaic Materials: Cu_2ZnSnS_4 (CZTS) nanocrystals Synthesized via Industrially Scalable, Green, One- step Mechanochemical Process. *Prog. Photovolt. Res. Appl.* **2019,** *27*, 798-811. DOI:10.1002/pip.3152
69. Baláž, M.; Zorkovská, A.; Urakaev, F.; Baláž, P.; Briančin, J.; Bujňaková, Z.; Achimovičová, M.; Gock, E., Ultrafast Mechanochemical Synthesis of Copper Sulfides. *RSC Adv.* **2016,** *6* (91), 87836-87842. DOI: 10.1039/c6ra20588g
70. Achimovičová, M.; Dutková, E.; Tóthová, E.; Bujňaková, Z.; Briančin, J.; Kitazono, S., Structural and Optical Properties of Nanostructured Copper Sulfide Semiconductor Synthesized in an Industrial Mill. *Front. Chem. Sci. Eng.* **2019,** *13* (1), 164-170. DOI: 10.1007/s11705-018-1755-2
71. Baláž, M.; Bujňáková, Z.; Achimovičová, M.; Tešinský, M.; Baláž, P., Simultaneous Valorization of Polyvinyl Chloride and Eggshell Wastes by a Semi-industrial Mechanochemical Approach. *Environ. Res.* **2019,** *170*, 332-336. DOI: 10.1016/j.envres.2018.12.005

72. de Chalbaud, L.; Delgado, J.; Sagredo, V.; Tomlinson, R.; Hill, A.; Pilkington, R., X-ray Powder Diffraction Data and Structural Characterization of Cu_2GeS_3 and Cu_2SnS_3. *Ternary and Multinary Comp.* **1998,** *152*, 151-154.
73. Palatnik, L.; Komnik, I.; Koshkin, V.; Belova, E., A Group of Ternary Semiconducting Compounds. *Doklady Akademii Nauk SSSR* **1961,** *137* (1), 68-71.
74. Oliva, F.; Arques, L.; Acebo, L.; Guc, M.; Sanchez, Y.; Alcobe, X.; Perez-Rodriguez, A.; Saucedo, E.; Izquierdo-Roca, V., Characterization of Cu_2SnS_3 Polymorphism and its Impact on Optoelectronic Properties. *J. Mater. Chem. A* **2017,** *5* (45), 23863-23871. DOI: 10.1039/c7ta08705e
75. Suekuni, K.; Tsuruta, K.; Ariga, T.; Koyano, M., Thermoelectric Properties of Mineral Tetrahedrites $Cu_{10}Tr_2Sb_4S_{13}$ with Low Thermal Conductivity. *Appl. Phys. Express* **2012,** *5*, 051201-3. DOI: 10.1143/APEX.5.051201
76. Chetty, R.; Bali, A.; Mallik, R., Tetrahedrites as Thermoelectric Materials: an Overview. *J. Mater. Chem. C* **2015,** *3* (48), 12364-12378. DOI: 10.1039/c5tc02537k
77. Baláž, P.; Guilmeau, E.; Daneu, N.; Dobrozhan, O.; Baláž, M.; Hegeduš, M.; Barbier, T.; Achimovičová, M.; Kaňuchová, M.; Briančin, J., Tetrahedrites Synthesized via Scalable Mechanochemical Process and Spark Plasma Sintering. *J. Eur. Ceram. Soc.* **2020,** *40*, 1922-1930. DOI: 10.1016/j.jeurceramsoc.2020.01.023
78. Barbier, T.; Lemoine, P.; Gascoin, S.; Lebedev, O.; Kaltzoglou, A.; Vaqueiro, P.; Powell, A.; Smith, R.; Guilmeau, E., Structural Stability of the Synthetic Thermoelectric Ternary and Nickel-substituted Tetrahedrite Phases. *J. Alloy. Compd.* **2015,** *634*, 253-262. DOI: 10.1016/j.jallcom.2015.02.045
79. Wang, L.; Yang, B.; Xia, Z.; Leng, M.; Zhou, Y.; Xue, D.; Zhong, J.; Gao, L.; Song, H.; Tang, J., Synthesis and Characterization of Hydrazine Solution Processed $Cu_{12}Sb_4S_{13}$ film. *Sol. Energ. Mat. Sol. C.* **2016,** *144*, 33-39. DOI: 10.1016/j.solmat.2015.08.016
80. Kumar, D.; Ren, M.; Osipowicz, T.; Mallik, R.; Malar, P., Tetrahedrite ($Cu_{12}Sb_4S_{13}$) Thin Films for Photovoltaic and Thermoelectric Applications. *Sol. Energ.* **2018,** *174*, 422-430. DOI: 10.1016/j.solener.2018.08.080
81. Guler, A.; Ballikaya, S.; Boyraz, C.; Okay, C.; Shulgin, D.; Rameev, B., Thermoelectric Properties and EPR Analysis of Fe Doped $Cu_{12}Sb_4S_{13}$. *J. Solid State Chem.* **2019,** *269*, 547-552. DOI: 10.1016/j.jssc.2018.10.019
82. Knížek, K.; Levinský, P.; Hejtmánek, J., LDA plus U Calculation of Electronic and Thermoelectric Properties of Doped Tetrahedrite $Cu_{12}Sb_4S_{13}$. *J. Electron. Mater.* **2019,** *48* (4), 2018-2021. DOI: 10.1007/s11664-019-06960-x
83. Kumar, D.; Tippireddy, S.; Ramakrishnan, A.; Chen, K.; Malar, P.; Mallik, R., Thermoelectric and Electronic Properties of Chromium Substituted Tetrahedrite. *Semicond. Sci. Tech.* **2019,** *34* (3), 035017. DOI: 10.1088/1361-6641/aafa31
84. Huang, L.; Kong, Y.; Zhang, J.; Xu, R.; Zhu, C.; Wu, J.; Jabbar, B.; Li, D.; Wang, Z.; Qin, X., Achieving a High Thermoelectric Performance of Tetrahedrites by Adjusting the Electronic Density of States and Enhancing Phonon Scattering. *ACS Appl. Mater. Inter.* **2019,** *11* (26), 23361-23371. DOI: 10.1021/acsami.9b06463
85. Tippireddy, S.; Kumar, D.; Karati, A.; Ramakrishnan, A.; Sarkar, S.; Peter, S.; Malar, P.; Chen, K.; Murty, B.; Mallik, R., Effect of Sn Substitution on the Thermoelectric Properties of Synthetic Tetrahedrite. *ACS Appl. Mater. Inter.* **2019,** *11* (24), 21686-21696. DOI: 10.1021/acsami.9b02956
86. Kumar, D.; Chetty, R.; Rogl, P.; Rogl, G.; Bauer, E.; Malar, P.; Mallik, R., Thermoelectric Properties of Cd Doped Tetrahedrite: $Cu_{12-x}Cd_xSb_4S_{13}$. *Intermetallics* **2016,** *78*, 21-29. DOI: 10.1016/j.intermet.2016.08.003

87. Ohtaki, M.; Koga, H.; Tokunaga, T.; Eguchi, K.; Arai, H., Electrical-transport Properties and High-temperature Thermoelectric Performance of Ca(0.9)M(0.1))MnO3 (M=Y,La,Ce,Sm,In,Sn,Sb,Pb,Bi). *J. Solid State Chem.* **1995,** *120* (1), 105-111. DOI: 10.1006/jssc.1995.1384
88. Chetty, R.; Bali, A.; Naik, M.; Rogl, G.; Rogl, P.; Jain, M.; Suwas, S.; Mallik, R., Thermoelectric Properties of Co Substituted Synthetic Tetrahedrite. *Acta Mater.* **2015,** *100*, 266-274. DOI: 10.1016/j.actamat.2015.08.040
89. Chetty, R.; Kumar, D.; Rogl, G.; Rogl, P.; Bauer, E.; Michor, H.; Suwas, S.; Puchegger, S.; Giester, G.; Mallik, R., Thermoelectric Properties of a Mn Substituted Synthetic Tetrahedrite. *Phys. Chem. Chem. Phys.* **2015,** *17* (3), 1716-1727. DOI: 10.1039/c4cp04039b
90. Narjis, A.; Outzourhit, A.; Aberkouks, A.; El Hasnaoui, M.; Nkhaili, L., Structural and Thermoelectric Properties of Copper Sulphide Powders. *J. Semicond.* **2018,** *39* (12), 122001-5. DOI: 10.1088/1674-4926/39/12/122001
91. Baláž, P.; Sekula, F.; Jakabský, Š.; Kammel, R., Application of Attrition Grinding in Alkaline Leaching of Tetrahedrite. *Miner. Eng.* **1995,** *8* (11), 1299-1308. DOI: 10.1016/0892-6875(95)00097-A
92. Lu, X.; Morelli, D.; Xia, Y.; Zhou, F.; Ozolins, V.; Chi, H.; Zhou, X.; Uher, C., High Performance Thermoelectricity in Earth-Abundant Compounds Based on Natural Mineral Tetrahedrites. *Adv. Ener. Mater.* **2013,** *3* (3), 342-348. DOI: 10.1002/aenm.201200650
93. Lu, X.; Morelli, D., Natural Mineral Tetrahedrite as a Direct Source of Thermoelectric Materials. *Phys. Chem. Chem. Phys.* **2013,** *15* (16), 5762-5766. DOI: 10.1039/c3cp50920f
94. Lu, X.; Morelli, D., Rapid Synthesis of High-performance Thermoelectric Materials Directly from Natural Mineral Tetrahedrite. *MRS Commun.* **2013,** *3* (3), 129-133. DOI: 10.1557/mrc.2013.26
95. Ge, Z. H.; Zhang, Y. X.; Song, D.; Chong, X.; Qin, P.; Zheng, F.; Feng, J.; Zhao, L. D., Excellent *ZT* Achieved in $Cu_{1.8}S$ Thermoelectric Alloys through Introducing Rare-earth Trichlorides. *J. Mater. Chem. A* **2018,** *6* (29), 14440-14448. DOI:0.1039/C8TA03195A
96. Qin, P.; Qian, X.; Ge, Z.; Zheng, L.; Feng, J.; Zhao, L., Improvements of Thermoelectric Properties for p-type $Cu_{1.8}S$ Bulk Materials via Optimizing the Mechanical Alloying Process. *Inorg. Chem. Front.* **2017,** *4* (7), 1192-1199. DOI: 10.1039/c7qi00208d
97. Zhang, R.; Chen, K.; Du, B.; Reece, M., Screening for Cu-S Based Thermoelectric Materials Using Crystal Structure Features. *J. Mater. Chem. A* **2017,** *5* (10), 5013-5019. DOI: 10.1039/c6ta10607b
98. Siloi, I.; Gopal, P.; Curtarolo, S.; Nardelli, M.; Vaqueiro, P.; Fornari, M., Thermoelectric Properties of Minerals with the Mawsonite Structure. *ACS Appl. Energ. Mater.* **2019,** *2* (11), 8068-8078. DOI: 10.1021/acsaem.9b01564
99. Baláž, P.; Hegeduš, M.; Reece, M.; Zhang, R.; Su, T.; Škorvánek, I.; Briančin, J.; Baláž, M.; Mihálik, M.; Tešinský, M.; Achimovičová, M., Mechanochemistry for Thermoelectrics: Nanobulk $Cu_6Fe_2SnS_8/Cu_2FeSnS_4$ Composite Synthesized in an Industrial Mill. *J. Electron. Mater.* **2019,** *48* (4), 1846-1856. DOI: 10.1007/s11664-019-06972-7
100. Suekuni, K.; Kim, F.; Nishiate, H.; Ohta, M.; Tanaka, H.; Takabatake, T., High-performance Thermoelectric Minerals: Colusites $Cu_{26}V_2M_6S_{32}$ (M = Ge, Sn). *Appl. Phys. Lett.* **2014,** *105*, 132107. DOI: 10.1063/1.4896998
101. Bourges, C.; Bouyrie, Y.; Supka, A.; Al Orabi, R.; Lemoin, P.; Lebedev, O.; Ohta, M.; Suekuni, K.; Nassif, V.; Hardy, V.; Daou, R.; Miyazaki, Y.; Fornari, M.; Guilmeau, E., High-Performance Thermoelectric Bulk Colusite by Process Controlled Structural Disordering. *J. Am .Chem. Soc.* **2018,** *140* (6), 2186-2195. DOI: 10.1021/jacs.7b11224
102. Dobrozhan, O.; Baláž, M.; Vorobiov, S.; Baláž, P.; Opanasyuk, A., Morphological, Structural, Optical Properties and Chemical Composition of Flexible Cu_2ZnSnS_4 Thin Films

Obtained by Ink-jet Printing of Polyol-mediated Nanocrystals. *J. Alloy. Compd.* **2020,** *842*, 155883. DOI:10.1016/j.jallcom.2020.155883

103. Nagaoka, A.; Masuda, T.; Yasui, S.; Taniyama, T.; Nose, Y., The Single-crystal Multinary Compound Cu_2ZnSnS_4 as an Environmentally Friendly High-performance Thermoelectric Material. *Appl. Phys. Express* **2018,** *11*(5). DOI: 10.7567/APEX.11.051203
104. Jiang, Q.; Yan, H.; Lin, Y.; Shen, Y.; Yang, J.; Reece, M., Colossal Thermoelectric Enhancement in $Cu_{2+x}Zn_{1-x}SnS_4$ Solid Solution by Local Disordering of Crystal Lattice and Multi-scale Defect Engineering. *J. Mater. Chem. A* **2020,** *8* (21), 10909-10916. DOI: 10.1039/d0ta01595d
105. Baláž, P.; Hegeduš, M.; Achimovičová, M.; Baláž, M.; Tešinský, M.; Dutková, E.; Kaňuchová, M.; Briančin, J., Semi-industrial Green Mechanochemical Syntheses of Solar Cell Absorbers Based on Quaternary Sulfides. *ACS Sustain. Chem. Eng.* **2018,** *6* (2), 2132-2141. DOI: 10.1021/acssuschemeng.7b03563
106. Liu, M.; Huang, F.; Chen, L.; Chen, I., A Wide-band-gap p-type Thermoelectric Material Based on Quaternary Chalcogenides of Cu(2)ZnSnQ(4) (Q=S,Se). *Appl. Phys. Lett.* **2009,** *94*, 202103-3. DOI: 10.1063/1.3130718
107. Ritscher, A.; Hoelzel, M.; Lerch, M., The Order-Disorder Transition in Cu_2ZnSnS_4-A Neutron Scattering Investigation. *J. Solid State Chem.* **2016,** *238*, 68-73. DOI: 10.1016/j.jssc.2016.03.013
108. Quennet, M.; Ritscher, A.; Lerch, M.; Paulus, B., The Order-Disorder Transition in Cu_2ZnSnS_4: A Theoretical and Experimental Study. *J Solid State Chem* **2017,** *250*, 140-144. DOI: 10.1016/j.jssc.2017.03.018
109. Isotta, E.; Fanciulli, C.; Pugno, N.; Scardi, P., Effect of the Order-Disorder Transition on the Seebeck Coefficient of Nanostructured Thermoelectric Cu_2ZnSnS_4. *Nanomater.* **2019,** *9*, 762. DOI: 10.3390/nano9050762
110. Chen, K.; Di Paola, C.; Laricchia, S.; Reece, M. J.; Weber, C.; McCabe, E.; Abrahams, I.; Bonini, N., Structural and Electronic Evolution in the Cu_3SbS_4–Cu_3SnS_4 Solid Solution. *J. Mater. Chem. C* **2020,** *8*, 11508-11516. DOI:10.1039/D0TC01804J

"For Table of Contents Only"

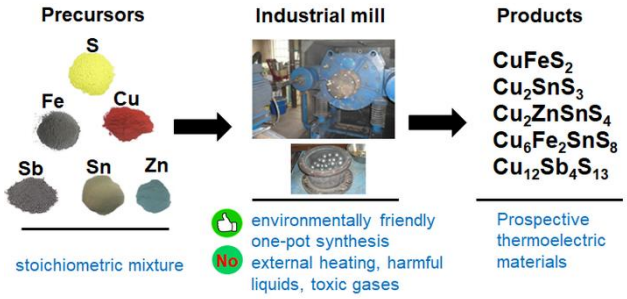

One-step solid-state scalable mechanochemical approach applying elements as precursors for the synthesis of multinary sulfides and their thermoelectric performance is reported herein.